

Relationship between self-propelled velocity and Brownian motion for spherical and ellipsoid particles

Jingwen Wang(汪静文), Ming Xu(徐明), and Deming Nie(聂德明)

Citation: Chin. Phys. B, 2024, 33 (**11**): 114601. DOI: 10.1088/1674-1056/ad7727
Journal homepage: http://cpb.iphy.ac.cn; http://iopscience.iop.org/cpb

What follows is a list of articles you may be interested in

Collective motion of polar active particles on a sphere

Yi Chen(陈奕), Jun Huang(黄竣), Fan-Hua Meng(孟繁华), Teng-Chao Li(李腾超), and Bao-Quan Ai(艾保全)
Chin. Phys. B, 2021, 30 (**10**): 100510. DOI: 10.1088/1674-1056/abfccf

Migration and shape of cells on different interfaces

Xiaochen Wang(王晓晨), Qihui Fan (樊琪慧), and Fangfu Ye(叶方富)
Chin. Phys. B, 2021, 30 (**9**): 090502. DOI: 10.1088/1674-1056/abf557

Active Brownian particles simulated in molecular dynamics

Liya Wang(王丽雅), Xinpeng Xu(徐新鹏), Zhigang Li(李志刚), Tiezheng Qian(钱铁铮)
Chin. Phys. B, 2020, 29 (**9**): 090501. DOI: 10.1088/1674-1056/aba60d

Anomalous boundary deformation induced by enclosed active particles

Wen-De Tian(田文得), Yan Gu(顾燕), Yong-Kun Guo(郭永坤), Kang Chen(陈康)
Chin. Phys. B, 2017, 26 (**10**): 100502. DOI: 10.1088/1674-1056/26/10/100502

An image encryption scheme based on three-dimensional Brownian motion and chaotic system

Xiu-Li Chai(柴秀丽), Zhi-Hua Gan(甘志华), Ke Yuan(袁科), Yang Lu(路杨), Yi-Ran Chen(陈怡然)
Chin. Phys. B, 2017, 26 (**2**): 020504. DOI: 10.1088/1674-1056/26/2/020504

Relationship between self-propelled velocity and Brownian motion for spherical and ellipsoid particles

Jingwen Wang(汪静文), Ming Xu(徐明), and Deming Nie(聂德明)†

College of Metrology Measurement and Instrument, China Jiliang University, Hangzhou 310018, *China*

(Received 18 July 2024; revised manuscript received 26 August 2024; accepted manuscript online 4 September 2024)

The Brownian motion of spherical and ellipsoidal self-propelled particles was simulated without considering the effect of inertia and using the Langevin equation and the diffusion coefficient of ellipsoidal particles derived by Perrin. The Péclet number (*Pe*) was introduced to measure the relative strengths of self-propelled and Brownian motions. We found that the motion state of spherical and ellipsoid self-propelled particles changed significantly under the influence of Brownian motion. For spherical particles, there were three primary states of motion: 1) when $Pe < 30$, the particles were still significantly affected by Brownian motion; 2) when $Pe > 30$, the self-propelled velocities of the particles were increasing; and 3) when $Pe > 100$, the particles were completely controlled by the self-propelled velocities and the Brownian motion was suppressed. In the simulation of the ellipsoidal self-propelled particles, we found that the larger the aspect ratio of the particles, the more susceptible they were to the influence of Brownian motion. In addition, the value interval of *Pe* depended on the aspect ratio. Finally, we found that the directional motion ability of the ellipsoidal self-propelled particles was much weaker than that of the spherical self-propelled particles.

Keywords: Brown motion, self-propelled particle, orientation movement

PACS: 46.65.+g, 05.40.Jc, 47.27.ek, 05.10.Gg **DOI:** 10.1088/1674-1056/ad7727

1. Introduction

Brownian motion is the phenomenon of the random thermal motion of molecules at the microscopic level.[1] The sizes of particles in Brownian motion are usually on the scale of micrometers or smaller, and only smaller molecules exhibit an unbalanced state due to collisions with surrounding medium-sized molecules.[2] For a long time, Brownian motion has been a significant research topic and has always garnered widespread interest in theoretical research fields such as statistical climate dynamics,[3] molecular motion theory[4] and thermodynamics.[5,6] In recent years, Brownian motion has also been fully developed in application-oriented fields such as traffic flow,[7] finance and economics[8] and nanomaterials.[9] Due to the profound research significance of Brownian motion, scholars have not only performed theoretical experiments,[10–16] but have also conducted simulations[17–20] and engaged in joint experimental and simulation studies.[21]

Traditional numerical methods used to study Brownian motion are primarily Stokes dynamics[22] and Brownian dynamics.[23] The motion of Brownian particles is usually decomposed into the two components of fluid motion and particle motion, which are modeled using the Navier–Stokes equations and the Langevin equation,[24] respectively. The most common method of studying Brownian motion is to examine the effect of Brownian motion and thermophoresis on heat transfer in nanofluids.[25–28] The Brownian motion of active particles in different media in various types of flow fields has also been investigated.[29–33] Furthermore, the Brownian motion of active particles affected by external forces in different electric, magnetic and thermal radiation environments has been analyzed.[34–37] In many studies, Brownian motion is usually considered a minor influencing factor rather than a major one. Moreover, because of the limitations of experiments and simulations, the study of anisotropic ellipsoidal particles is usually confined to the two-dimensional or quasi-two-dimensional region,[38–44] which hinders thorough investigation into the extent to which Brownian motion exerts a qualitative influence on the motion of micro- and nanoparticles.

In order to fill the research gap in this field, Brownian motion and the coupled motion of micro- and nanoparticles have been deeply explored. Therefore, our study analyzes the Brownian motion of micro- and nanoparticles in an unrestricted region without considering inertial influences, and excluding other influencing factors. In this case, the effect of Brownian motion on the motion of spherical and ellipsoidal self-driven particles in three-dimensional space is evaluated. This will visualize the relationship between random and directional motions of self-driven particles, which will play an important role in providing guidance for the directional transport of nanodevices. Perrin[45,46] calculated the translational friction and rotational friction coefficients of the ellipsoid using Oberbeck's method[47] and Edwardes' method,[48] respectively. We apply the formulae derived by Perrin and combine them with the Langevin equation to simulate the stochastic motions of common spherical and ellipsoidal self-driven parti-

†Corresponding author. E-mail: nieinhz@cjlu.edu.cn

© 2024 Chinese Physical Society and IOP Publishing Ltd

cles, respectively, compare the spherical and ellipsoidal particles and analyze the ellipsoidal particles with different length-to-diameter ratios. The strength of the self-driven velocity and random motion of the particles is analyzed by referencing the Péclet number (*Pe*),[49] which enables a quantitative comparison of the results of the study. The results of this study offer important insight into the qualitative and quantitative analysis of the random motion characteristics of micro- and nanoparticles. This enables the strength relationship between self-propelled and random motions to be analyzed, which can form the basis of an important theoretical guideline for the application of micro- and nanoparticles and resistance to Brownian motion.

The rest of this paper is organized as follows. Section 2 introduces the numerical method, Section 3 describes the validation of the model, Section 4 discusses and analyzes the simulation results, and Section 5 contains the conclusions of the study.

2. Numerical method

In Brownian motion, the forces acting on the particles according to the Langevin equation[23] are usually categorized as Brownian forces and fluid resistance. In our simulations, there were no inertial influences, and the translational and rotational motions of the passive particles in a homogeneous medium were independent of each other. For spherical particles, the translational diffusion coefficient is denoted as D_{T} and the rotational diffusion coefficient is denoted as D_{R}, which are defined as

$$D_{\mathrm{T}}=\frac{k_{\mathrm{B}}T}{6\pi\eta R},\quad D_{\mathrm{R}}=\frac{k_{\mathrm{B}}T}{8\pi\eta R^{3}}, \tag{1}$$

where k_{B} is the Boltzmann constant, T denotes the temperature, η represents the fluid viscosity and R denotes the spherical radius. Therefore, the translational and rotational stochastic equations of motion for spherical passive Brownian particles in three dimensions are

$$\begin{cases}\dot{x}=\sqrt{2D_{\mathrm{T}}}\xi_x,\\ \dot{y}=\sqrt{2D_{\mathrm{T}}}\xi_y,\\ \dot{z}=\sqrt{2D_{\mathrm{T}}}\xi_z,\end{cases}\quad\begin{cases}\dot{\varphi}=\sqrt{2D_{\mathrm{R}}}\xi_\varphi,\\ \dot{\phi}=\sqrt{2D_{\mathrm{R}}}\xi_\phi,\\ \dot{\psi}=\sqrt{2D_{\mathrm{R}}}\xi_\psi,\end{cases} \tag{2}$$

where $\dot{x}$, $\dot{y}$ and $\dot{z}$ denote the translational position and direction of the particle, ξ_x, ξ_y, and ξ_z are zero-mean Gaussian noise random numbers used for modeling the random effects of Brownian motion in the translational direction, $\dot{\varphi}$, $\dot{\phi}$ and $\dot{\psi}$ denote the different rotational directions of the particles and ξ_φ, ξ_ϕ and ξ_ψ are zero-mean Gaussian noise random numbers used for simulating the stochastic effects of Brownian motion in the rotational direction. Each equation is decoupled from every other equation.

For a self-propelled particle with velocity U, the rotational diffusive motion is the same as that of a passive spherical particle. However, the direction of the translational motion itself is affected by the rotational diffusion. In this case, the translation and rotation of self-propelled particles are correlated, and the corresponding translational equations of motion are

$$\begin{cases}\dot{x}=U\cos\varphi+\sqrt{2D_{\mathrm{T}}}\xi_x,\\ \dot{y}=U\cos\phi+\sqrt{2D_{\mathrm{T}}}\xi_y,\\ \dot{z}=U\cos\psi+\sqrt{2D_{\mathrm{T}}}\xi_z.\end{cases} \tag{3}$$

Unlike spherical particles, ellipsoidal particles are an important class of anisotropic particles. Perrin[45,46] calculated the translational friction and rotational friction coefficients of the ellipsoid using Oberbeck's method[47] and Edwardes' method,[48] respectively. The translational friction and rotational friction coefficients are expressed as

$$\begin{aligned}f_1&=\frac{16\pi\eta\left(a^2-b^2\right)}{\left(2a^2-b^2\right)S-2a},\\ f_2=f_3&=\frac{32\pi\eta\left(a^2-b^2\right)}{\left(2a^2-b^2\right)S+2a},\end{aligned} \tag{4a}$$

$$\begin{aligned}G_1&=\frac{32\pi\eta\left(a^2-b^2\right)b^2}{3\left(2a-b^2S\right)},\\ G_2=G_3&=\frac{32\pi\eta\left(a^4-b^4\right)}{3\left(2a-b^2S\right)-2a},\end{aligned} \tag{4b}$$

where f_1 denotes the translational friction coefficient of the ellipsoid along the long axis, $f_2=f_3$ denotes the translational friction coefficient of the ellipsoid along the short axis, G_1 denotes the rotational friction coefficient of the ellipsoid rotating along the long axis, $G_2=G_3$ denotes the rotational friction coefficient of the ellipsoid rotating along the short axis, a denotes the long semi-axis of the ellipsoid, $b=c$ denotes the two equal short semi-axes of the ellipsoid, $\beta=a/b$ denotes the aspect ratio of the ellipsoidal particles, and S is the coefficient related to the ellipsoid aspect ratio

$$\begin{cases}S=\dfrac{2}{\sqrt{a^2-b^2}}\log\dfrac{a+\sqrt{a^2-b^2}}{b}, & (a>b=c),\\ S=\dfrac{2}{\sqrt{b^2-a^2}}\tan^{-1}\left(\dfrac{\sqrt{b^2-a^2}}{a}\right), & (a<b=c).\end{cases} \tag{5}$$

Using the translational and rotational friction coefficients of the ellipsoid in each direction, we obtain the translational and rotational diffusion coefficients of the ellipsoid. The translational diffusion coefficient along the long axis is denoted as $D_{\parallel}$ and the translational diffusion coefficient along the two short axes is denoted as $D_{\perp}$, and they are defined as

$$D_{\parallel}=\frac{k_{\mathrm{B}}T}{f_1},\quad D_{\perp}=\frac{k_{\mathrm{B}}T}{f_2}. \tag{6}$$

The rotational diffusion coefficient around the long axis is denoted as $D_{\mathrm{R}\parallel}$ and the rotational diffusion coefficient around the two short axes is denoted as $D_{\mathrm{R}\perp}$, and they are defined as

$$D_{\mathrm{R}\parallel}=\frac{k_{\mathrm{B}}T}{G_1},\quad D_{\mathrm{R}\perp}=\frac{k_{\mathrm{B}}T}{G_2}. \tag{7}$$

Based on the diffusion coefficients in each direction, the overall translational and rotational diffusion coefficients of the ellipsoid can be expressed as

$$D_{\mathrm{ET}} = \frac{D_{\parallel} + 2D_{\perp}}{3}, \quad D_{\mathrm{ER}} = \frac{D_{\mathrm{R}\parallel} + 2D_{\mathrm{R}\perp}}{3}. \tag{8}$$

The passive and self-propelled motion equations for ellipsoidal particles are the same as those for spherical particles except for the diffusion coefficient, as indicated by a comparison between Eqs. (2) and (3).

Due to the different diffusion coefficients for spherical and ellipsoidal particles, the Péclet number (*Pe*) [44] is calculated differently. For spherical particles, *Pe* is calculated as

$$Pe = \frac{U}{\sqrt{D_{\mathrm{T}} D_{\mathrm{R}}}}. \tag{9}$$

For ellipsoidal particles, *Pe* is calculated as

$$Pe = \frac{U}{\sqrt{D_{\mathrm{ET}} D_{\mathrm{ER}}}}. \tag{10}$$

3. Validation

In the process of constructing the model, we chose the classical mode of the Langevin equation. The influence of inertia was not considered in the simulation process, and the particles moved in the unrestricted region. The process of Brownian motion was simulated via direct action on the particles themselves. To simplify the simulation, the parameters of the particles were set as $k_{\mathrm{B}}T = 1$, $T = 0.01$, $\eta = 0.1$ and $R = 6$ for the spherical particles, and this is relatively common in direct numerical simulations. We used Eq. (1) to calculate D_{T} and D_{R} for the spherical particles. Figure 1 shows a diagram of the trajectory of a single passive spherical particle, which is disorderly and irregular (consistent with Brownian motion). The data were quantitatively verified according to Einstein's diffusion formula, and the mean squared displacement of the translational was verified, as shown in Fig. 1(b). Because a three-dimensional sphere was simulated, the coefficients of the fitting data shown in Fig. 1(b) were $6D_{\mathrm{T}}$. The data were quantitatively verified according to Einstein's diffusion formula, and the mean squared displacement of the rotational was verified, as shown in Fig. 2. Because a three-dimensional sphere was simulated, the coefficients of the fitting data shown in Fig. 2 were $6D_{\mathrm{R}}$. The fitting results also verified the accuracy of the Brownian motion model of the spherical particle.

After the simulation of the spherical particles was verified, we also verified the simulation of ellipsoidal particles with $\beta = 2$. Ellipsoidal particles have a long semi-axis ($a = 12$) and short semi-axis ($b = c = 6$). We used Eqs. (4)–(8) to calculate D_{ET} and D_{ER} for the ellipsoidal particles. Figure 3(a) shows a diagram of the trajectory of the ellipsoidal passive particles. The trajectories of the particles were quantitatively analyzed, as shown in Fig. 3(b). The fitting data coefficients of the translational are $6D_{\mathrm{ET}}$. In Fig. 4, the fitting data coefficients of the rotational was $6D_{\mathrm{ER}}$. In addition, we further verified the Perrin formula. As shown in Fig. 5(a), the translational friction coefficient linearly increased as the length-diameter ratio of the ellipsoid increased. Moreover, Fig. 5(b) shows that the ratio of the translational diffusion coefficient for the ellipsoidal particles along the major axis to that along the minor

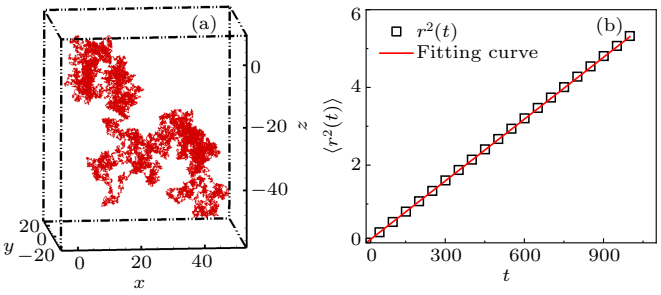


Fig. 1. (a) Trajectories of a single passive spherical particle. (b) Mean squared displacement of the passive spherical particles.

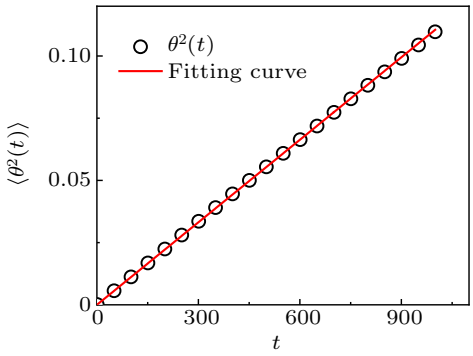


Fig. 2. Mean squared angular displacement of the passive spherical particles.

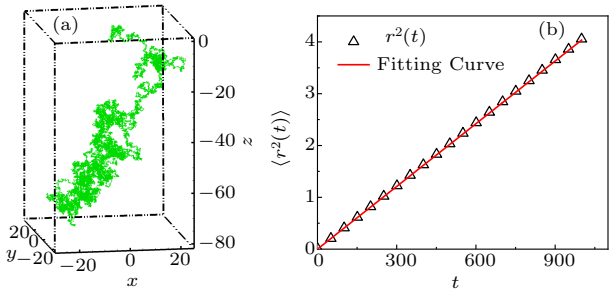


Fig. 3. (a) Trajectories of a single passive ellipsoid particle with $\beta = 2$. (b) Mean squared displacement of the passive ellipsoid particles.

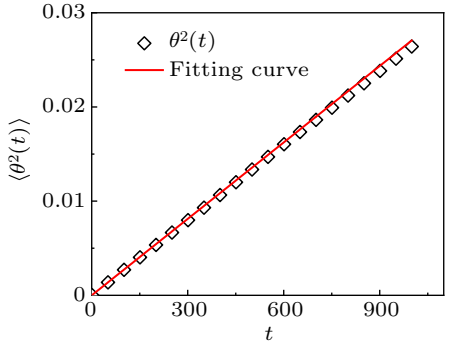


Fig. 4. Mean squared angular displacement of the passive ellipsoid particles.

axis grows as β increases. Theoretically, this ratio is equal to 2 for an infinitely elongated ellipsoid particle.[50] These quantitative analyses validated the model verification of the ellipsoidal particles.

The diffusivities of the ellipsoid particles were also different from those of the spherical particles because of the different length-diameter ratio. When other conditions did not change, the diffusion strengths of the passive ellipsoidal particles with different β values were also different. Figure 6(a) shows that the diffusion tracks of the ellipsoidal particles with different β values were slightly different. Passive ellipsoid particles with larger β values had smaller diffusion ranges, while particles with smaller β values had larger diffusion ranges. As shown in Fig. 6(b), we quantitatively analyzed the mean squared displacement of the ellipsoidal particles with different β values. The passive diffusion ability of particles with larger β values was worse, which was consistent with the linear relationship between the translational friction coefficient for ellipsoidal particles and β, as shown in Fig. 5(a).

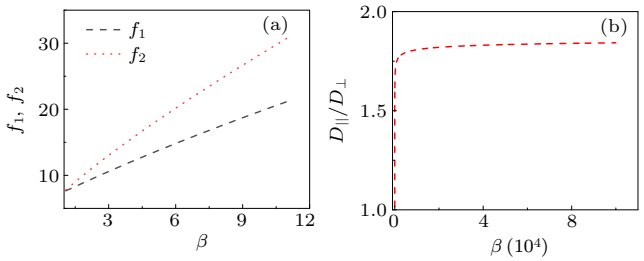


Fig. 5. (a) Verification of the relationship between the translational friction coefficient for ellipsoid particles and β. (b) Verification of the relationship between the translational diffusion coefficient for ellipsoid particles and β.

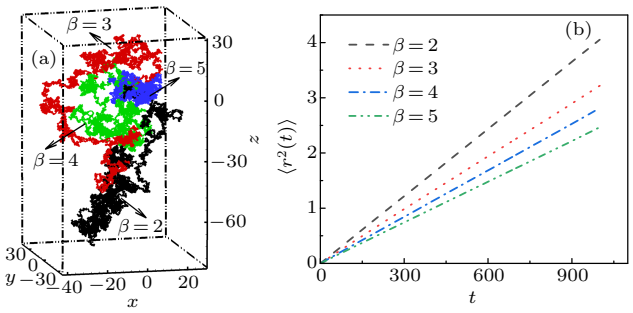


Fig. 6. (a) Trajectories of a single passive ellipsoid particle with different values of β. (b) Mean squared displacement of the passive ellipsoid particle for different values of β.

4. Results

4.1. Single active spherical Brownian particle

After the simulation of the passive spherical particles was validated, we simulated a self-propelled spherical particle. The coupling between the self-propelled velocity and Brownian motion of the spherical particle was examined. We investigated how the trajectory and mean squared displacement of the self-propelled spherical particle changed with different values of *Pe*. Figure 7 shows the calculation results of the trajectory and mean squared displacement of the spherical self-propelled particles at low values of *Pe*. Figure 7(a) indicates that the larger the value of *Pe*, the less obvious the trajectory fluctuation caused by the influence of Brownian motion of the particle, and the larger the overall range of motion of the particle. In the quantitative analysis shown in Fig. 7(b), the coefficient of the fitting data is $6D_{\mathrm{T}}$ when the passive diffusion of the spherical particle was verified. This is used to represent the mean squared displacement of the passive particle in the ideal state. According to the results shown in Fig. 7(b), the mean squared displacement of the particle was still linear at low values of *Pe*. However, as *Pe* increased, the mean squared displacement became nonlinear. As shown in Fig. 8(a), for high values of *Pe*, the self-propelled velocity of the dominant particle and the influence of Brownian motion are not obvious, so the trajectory of the particle is relatively smooth and the range of particle trajectory is large. In the quantitative analysis shown in Fig. 8(b), the calculated results of the mean squared displacement of the particles gradually tend to be in the form of a quadratic function as the value of *Pe* increases. When the calculated results of the mean squared displacement of the particles are closer to the quadratic function, the motion mode of the particles tends to be more self-driven motion.

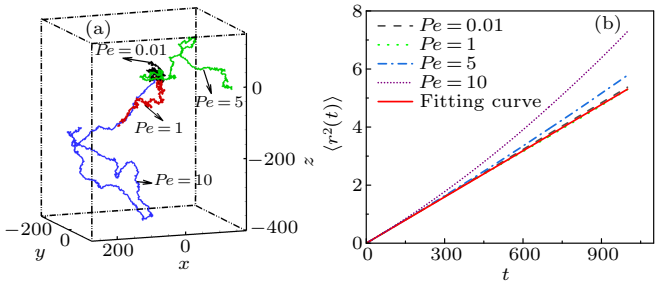


Fig. 7. (a) Trajectories of the active spherical particle at lower values of *Pe*. (b) Mean squared displacement of the active spherical particle at lower values of *Pe*.

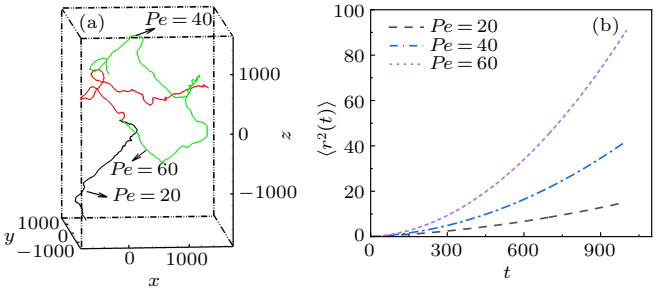


Fig. 8. (a) Trajectories of the active spherical particle at higher values of *Pe*. (b) Mean squared displacement of the active spherical particle at higher values of *Pe*.

To quantify the strength of the self-propelled velocity and random motion, the mean squared displacement of the particle for different *Pe* values was fitted to a power law as a function of t. By analyzing the fitting index α, the motion state of the

self-propelled particle was determined. As shown in Fig. 9, as the value of *Pe* increased, the fitting index reached a value of 2 during the growth process. This signified that traditional self-propelled motion dominated and Brownian motion was suppressed. In addition, according to the fitted values, when *Pe* is less than 30, the index value shows a trend of increasing, but when *Pe* is greater than 30, the exponential growth begins to decrease and tends to be stable, and when *Pe* is greater than 100, the index value basically no longer increases. Thus, when *Pe* was less than 30, the particle was still significantly affected by Brownian motion, and when *Pe* was greater than 30, the self-propelled motion of the particle began to be stronger than Brownian motion. When *Pe* was greater than 100, the particle was completely controlled by the self-propelled velocity, suppressing the Brownian motion.

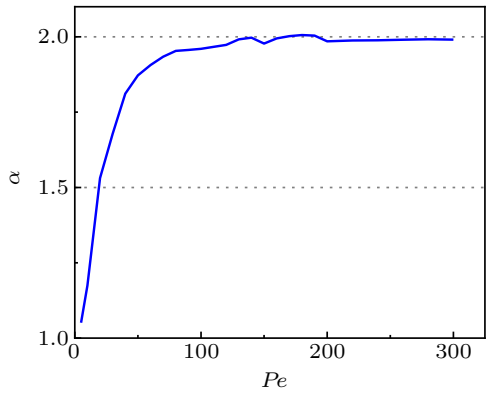


Fig. 9. Relationship between *Pe* and the mean squared displacement index of the self-propelled spherical particle.

4.2. Single active ellipsoidal Brownian particle

An ellipsoidal particle with $\beta = 2$ was selected to analyze the coupling effect between the self-propelled velocity and Brownian motion of a single ellipsoidal self-propelled particle. Figure 10 shows the calculation results of the trajectory and mean squared displacement of the self-propelled ellipsoid particle at low values of *Pe*. Figure 10(a) shows that the larger the value of *Pe*, the smaller the fluctuations of the particle's trajectory and the larger the range. In the quantitative analysis shown in Fig. 10(b), the coefficient of the fitting data is $6D_{\mathrm{ET}}$ when the passive diffusion of the spherical particle was verified. This is used to represent the mean squared displacement of the passive particle in the ideal state. According to the results shown in Fig. 10(b), the mean squared displacement of the particle was still linear at low values of *Pe*. However, as *Pe* increased, the mean squared displacement became nonlinear. As shown in Fig. 11(a), for high values of *Pe*, the trajectory of the particle was relatively smooth with a low degree of jitter and a larger trajectory range. In the quantitative analysis shown in Fig. 11(b), the mean squared displacement of the particle reflected the shape of a quadratic function towards pure self-propelled motion at high values of *Pe*.

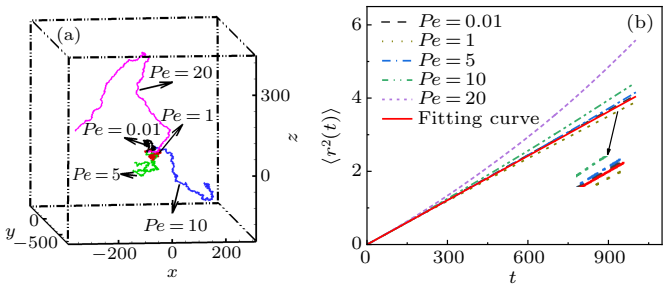


Fig. 10. (a) Trajectories of the active ellipsoid particle at lower values of *Pe*. (b) Mean squared displacement of the active ellipsoid particle at lower values of *Pe*.

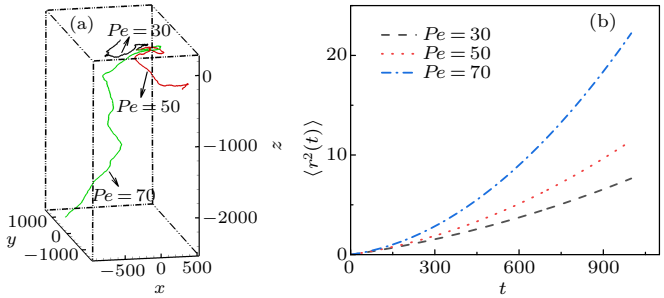


Fig. 11. (a) Trajectories of the active ellipsoid particle at higher values of *Pe*. (b) Mean squared displacement of the active ellipsoid particle at higher values of *Pe*.

We also fitted the mean squared displacement of the ellipsoidal self-propelled particles to a power law as a function of t for different *Pe* values. The results are shown in Fig. 12. As *Pe* increased, the fitting index approached a value of 2. In contrast to the spherical particle, the exponential growth of the ellipsoidal particle was not stable, exhibiting oscillations that prevented it from eventually stabilizing at a value of 2. This was caused by the anisotropy of the ellipsoid particle. The ellipsoid particle was not as stable as the spherical particle, and the diffusion coefficient of the ellipsoid particle was different on both the long and short axes. Thus, oscillations between states dominated by self-propelled motion and Brownian motion occurred.

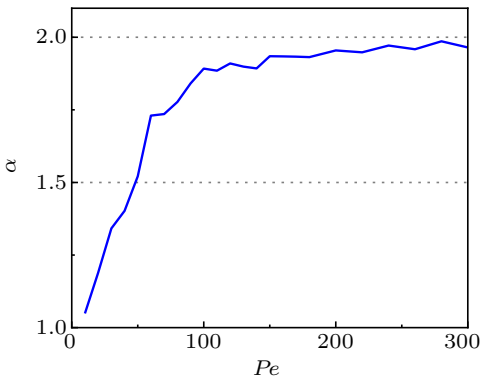


Fig. 12. Relationship between *Pe* and the mean squared displacement index of the self-propelled ellipsoid particle.

Figure 12 indicates that for the ellipsoidal particle, when *Pe* was less than 60, the particle was still significantly affected

by Brownian motion, but when *Pe* was greater than 60, the self-propelled velocity of the particle was increasing. When *Pe* was greater than 120, the particle was completely controlled by the self-propelled velocity, suppressing the Brownian motion. However, compared to the spherical self-propelled particle described in the previous section, the ellipsoidal self-propelled particle was more susceptible to Brownian motion.

4.3. Active ellipsoid Brownian particle at different aspect ratios

In the verification phase, we found that the diffusion coefficients of the ellipsoid particles with different aspect ratios were different. Therefore, in the analysis of the ellipsoidal self-propelled particle, we also simulated the motion of an ellipsoidal self-propelled particle for different values of β. Figure 13 shows the trajectories and mean squared displacement of the ellipsoidal self-propelled particle with different β values for the same *Pe* ($Pe = 100$). The trajectory diagram shown in Fig. 13(a) indicates that the trajectory range and oscillation amplitudes of the ellipsoidal particles with different values of β differed significantly. In addition, Fig. 13(b) shows that for the same *Pe* value, the larger the value of β, the higher the susceptibility of the ellipsoid particle to Brownian motion, and the lower the effect of self-propulsion. For further analysis, the mean squared displacement of the ellipsoidal particle with different values of β was fitted to a power law as a function of t for different *Pe* values, and the results are shown in Fig. 14. The figure shows that the α value of the ellipsoidal particle with different β values exhibited an increasing trend as *Pe* increased. However, the growth trends of the ellipsoidal particles with different β values were different, and the growth trends of α for the particles with larger β values were slower and more unstable. This demonstrates that under the same conditions, ellipsoidal particles with smaller values of β possess superior anti-Brownian motion characteristics and are capable of greater degrees of autonomous motion. This significant difference is related to the anisotropy of the ellipsoid particle. In the case of self-propelled particles, the translation and rotational diffusion of the ellipsoid are coupled. This exacerbates the instability of the motion of the ellipsoidal particles.

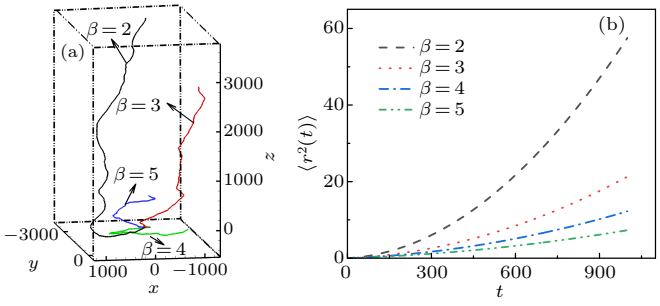


Fig. 13. (a) Trajectories of the active ellipsoid particle with different values of β for $Pe = 100$. (b) Mean squared displacement of the active ellipsoid particle for different values of β for $Pe = 100$.

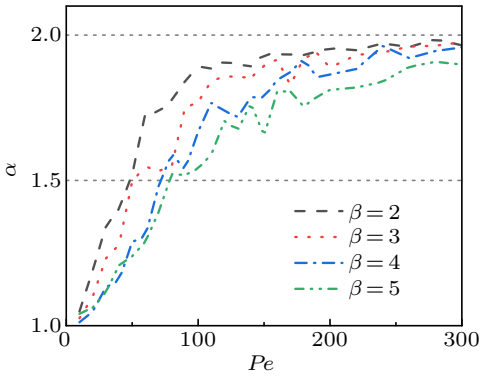


Fig. 14. Relationship between *Pe* and the mean squared displacement index of the self-propelled ellipsoid particle for different values of β.

5. Conclusion

By using the Langevin equation to simulate the motion states of spherical and ellipsoidal self-propelled particles under the influence of Brownian motion, we obtained the following conclusions.

(1) For spherical particles, when *Pe* was less than 30, the effect of Brownian motion on the particle was still dominant, and when *Pe* was greater than 30, the self-propelled velocity of the particle was dominant. When *Pe* was greater than 100, the particle was completely controlled by the self-propelled velocity, and the Brownian motion was suppressed. For ellipsoidal particles with small β ($\beta = 2$), when *Pe* was less than 60, the effect of Brownian motion on the particle was still dominant, and when *Pe* was greater than 60, the self-propelled velocity of the particle was dominant. When *Pe* was greater than 120, the particle was completely controlled by the self-propelled velocity.

(2) The self-propelled spherical particle resisted Brownian motion more effectively than the self-propelled ellipsoidal particle under the same conditions. For ellipsoidal particles, the smaller the β, the stronger the resistance to Brownian motion.

Our simulation is mainly restricted to particles without the influence of inertia. Furthermore, in the simulation, we explore what kind of different states of motion different-shaped particles will have under the influence of Brownian motion. The conclusions obtained provide insight into what types of effects Brownian motion can have on different shapes of particles. This plays an important role in guiding the design of modern microdevices, especially in the study of how to suppress Brownian motion.

Acknowledgements

Project supported by the National Natural Science Foundation of China (Grant Nos. 12372251 and 12132015) and the Fundamental Research Funds for the Provincial Universities of Zhejiang (Grant No. 2023YW69).

References

[1] Mörters P and Peres Y 2010 *Brownian motion* (1nd Edn.) (Redmond: Cambridge University Press) p. 416
[2] Genthon A 2020 *Eur. Phys. J. H* **45** 49
[3] Sonechkin D M 1998 *Int. J. Bifurcat. Chaos* **8** 799
[4] Cai C H, Hu J Q and Wang Y L 2021 *Fractal. Fractional* **5** 226
[5] Nie D and Lin J 2009 *Particuology* **7** 501
[6] Haq F, Khan M I, Khan S U, Abualnaja K M and El-Shorbagy M A 2022 *Chin. Phys. B* **31** 084703
[7] Shiftan Y, Button K and Nijkamp P 2007 *Transportation planning* (1nd Edn.) (Cheltenham: Edward Elgar Publishing) p. 672
[8] Dufera T T 2024 *N. Am. J. Econ. Financ* **69** 102017
[9] Kang M A, Fang J, Paragodaarachchi A Kodama K, Yakobashvili D, Ichiyanagi Y and Matsui H 2022 *Nano Lett.* **22** 8852
[10] Svetlov A S, Vasiliev M M, Kononov E A, Petrov O F and Trukhachev F M 2023 *Molecules* **28** 1790
[11] Svetlov A S, Kononov E A, Trukhachev F M, Vasiliev M M and Petrov O F 2023 *J. Exp. Theo. Phys.* **137** 615
[12] Villa S, Blanc C, Daddi-Moussa-Ider A, Stocco A and Nobili Maurizio 2023 *J. Colloid. Interface. Sci.* **629** 917
[13] Permpatdechakul T, Khajornrungruang P, Suzuki K, Blattler A and Inthiam J 2024 *Int. J. Auto. Tech. Jpn.* **18** 47
[14] Wang W, Metzler R and Cherstvy A G 2022 *Phys. Chem. Chem. Phys.* **24** 18482
[15] Boltnev R E, Vasiliev M M and Petrov O F 2023 *Sci. Rep.* **13** 22538
[16] Li Z K and Li D X 2023 *Chin. Phys. B* **32** 010203
[17] Hazarika S and Ahmed S 2022 *Math. Comput. Simulat.* **192** 452
[18] Kalpana G, Madhura K R and Kudenatti R B 2022 *Int. J. Eng. Sci.* **32** 101075
[19] Nie D and Lin J 2022 *J. Chem. Phys.* **157** 084102
[20] Xia Y Q, Feng G Q and Shen Z L 2022 *Chin. Phys. B* **31** 040204
[21] Zembrzycki K, Pawłowska S, Pierini F and Kowalewski T A 2023 *Polymers-basel* **15** 787
[22] Brady J F and Bossis G 1988 *Annu. Rev. Fluid. Mech* **20** 111
[23] Ermak D L and McCammon J A 1978 *J. Chem. Phys.* **69** 1352
[24] Langevin P 1908 *C R Hebd Seances Acad. Sci.* (Paris) **146** 530 (in French)
[25] Saleem S, Animasaun I L, Yook S J, Al-Mdallal Q M, Shah N A and Faisal M 2022 *Surf. Interfaces* **30** 101854
[26] Tawade J V, Guled C N, Noeiaghdam S, Fernandez-Gamiz U, Govindan V and Balamuralitharan S 2022 *Results in Engineering* **15** 100448
[27] Jalili P, Narimisa H, Jalili B, Shateri A and Ganji D D 2023 *Soft. Comput* **27** 677
[28] Samantaray S S, Misra A, Shaw S, Nayak M K, Nazari S, Boukhris I and Chamkha A J 2024 *Results in Engineering* **22** 101980
[29] Santra I, Basu U and Sabhapandit S 2021 *Phys. Rev. E* **104** L012601
[30] Zhu W J and Ai B Q 2022 *Chin. Phys. B* **31** 040503
[31] Alguacil F J and Alonso M 2024 *J. Aerosol. Sci.* **179** 106382
[32] Fukuda H, Kuramochi H, Shibuta Y and Ichiki T 2023 *APL Mach. Learn.* **1** 046104
[33] Iyaniwura S A and Peng Z 2024 *SIAM J. Appl. Math.* **84** 1079
[34] Ge-JiLe H, Shah N A, Mahrous Y M, Sharma P, Raju C S K and Upddhya S M 2021 *Case Stud. Therm. Eng.* **25** 100915
[35] Khan A, Ali I, Almusawa M Y, Gul T and Alghamdi W 2023 *Chin. Phys. B* **32** 084401
[36] Gao T F, Zheng Z G and Chen J C 2013 *Chin. Phys. B* **22** 080502
[37] Tapia-Ignacio C, Moctezuma R E, Donado F and Weeks E R 2020 *Phys. Rev. E* **102** 022902
[38] Cai R, Xiao H, Christov I C and Zhao Y 2021 *Aiche. J.* **67** e17109
[39] Li H H, Zheng Z Y and Wang Y R 2019 *Chin. Phys. Lett.* **36** 034701
[40] Mandal S and Anirban G 2023 arxiv:2308.03451 [cond-mat.soft]
[41] Zheng Z and Han Y 2010 *J. Chem. Phys.* **133** 124509
[42] Peng Y, Lai L, Tai Y S, Zhang K, Xu X and Cheng X 2016 *Phys. Rev. Lett.* **116** 068303
[43] Han Y, Alsayed A, Nobili M and Yodh A G 2009 arxiv:0903.1332 [cond-mat.soft]
[44] Li H H, Zheng Z Y and Wang Y R 2019 *Chin. Phys. Lett.* **36** 034701
[45] Perrin F 1934 *Phys. Radium* **5** 497 (in French)
[46] Perrin F 1936 *J. Phys. Radium* **7** 1 (in French)
[47] Oberbeck A 1876 *J. Reine. Angew. Math.* **81** 62 (in German)
[48] Edwardes D 1893 *Quart. J. Pure. Appl. Math.* **26** 270
[49] Bechinger C, Di Leonardo R, Löwen H, Reichhardt C, Volpe G and Volpe G 2016 *Rev. Mod. Phys.* **88** 045006
[50] Wang L, Lu Y and An L 2017 *Chin. J. Appl. Chem.* **34** 1250 (in Chinese)